IEEE Access
Multidisciplinary | Rapid Review | Open Access Journal

Received March 13, 2019, accepted April 8, 2019, date of current version April 29, 2019.

Digital Object Identifier 10.1109/ACCESS.2019.2911554

High-Resolution Imaging of Multi-Channel Forward-Looking Synthetic Aperture Radar Under Curve Trajectory

JINGYUE LU[1], LEI ZHANG[2], PENGFEI XIE[1], ZHICHAO MENG[1], AND YUNHE CAO[1]

[1]National Laboratory of Radar Signal Processing, Xidian University, Xi'an 710071, China
[2]School of Electronics and Communication Engineering, Sun Yat-sen University, Guangzhou 510275, China

Corresponding author: Lei Zhang (e-mail: leizhang@xidian.edu.cn)

This work was supported by the National Natural Science Foundation of China under Grant 61771372 and Grant 61771367.

ABSTRACT Forward-looking synthetic aperture radar is an essential tool in modern remote sensing applications, but its imaging is a challenging task. Few existing methods consider the curve trajectory. Aiming at the difficulty of resolution and the Doppler ambiguity in forward-looking SAR under the curve trajectory, this paper establishes a forward-looking multi-channel SAR system model and proposes a novel approach for the forward-looking SAR imaging under the curve trajectory. The approach is implemented by a two-step process: 1) The Doppler ambiguity under forward-looking mode is solved by adaptive beam-forming processing; and 2) A sparsity-driven optimization imaging algorithm is developed to enhance the azimuth angle resolution in the forward-looking direction, where the resolution gain aroused by the curve trajectory is exploited. The extensive simulation confirms the validity of the proposed approach.

INDEX TERMS SAR, forward-looking imaging, azimuth angle resolution, Doppler ambiguity, curve trajectory, sparsity-driven optimization

I. INTRODUCTION

Synthetic Aperture Radar (SAR) [1]– [4] has a wide range of applications in military reconnaissance and civilian remote sensing. At present, the main working modes of SAR are side-looking SAR, squint-looking SAR and spotlight SAR, which can be high-resolution two-dimensional imaging of scenes on both sides of the trajectory. Due to the constraint of SAR working principle, the existing SAR modes cannot image the area in front of the trajectory directly, which results in a forward-looking blind zone and therefore does not have front view high resolution capability. However, in applications such as precision guidance, complex terrain avoidance and battlefield reconnaissance, the high-resolution of the forward-looking SAR imaging is urgently needed. Forward-looking SAR imaging enables two-dimensional imaging of the front view of the platform. Compared with the traditional SAR, the forward-looking SAR imaging system has a strong coupling between azimuth and range, which makes the azimuth angle resolution difficult. In the meanwhile, there is an inherent Doppler ambiguity problem in forward-looking SAR imaging, that is, the symmetric targets on both sides of the trajectory have the same Doppler history. Nevertheless, forward-looking SAR imaging has to face the difficulties of the forward-looking resolution enhancement and the left-right Doppler ambiguity resolving simultaneously.

Moreover, due to the effect of platform vibration, wind field and turbulence, the platform might greatly deviate from the ideal trajectory. Compensation of the motion errors in forward-looking SAR [5] [6] is of great significance to achieve a well-focused image.

Up to now, the main techniques for tackling the problem of the conventional radar forward-looking blind zone can be divided into the following categories: (1) Forward-looking imaging technology for dense array SAR systems [7]–[9], which is representative of the Sector Imaging Radar for Enhanced Vision(SIREV) proposed by the German Space Agency. This system realizes two-dimensional imaging of the forward-looking area through forming a real aperture by use of a dense array in a vertical course direction. However, the system azimuth angle resolution is determined only by the real aperture of the array, that is, it is constrained by the physical size of the real aperture of the array, and the system tends to be rather complex. (2) Bistatic forward-looking SAR [10]–[15], which has been

The associate editor coordinating the review of this manuscript and approving it for publication was Anton Kos.

the focus of extensive research activity over the last decade. Firstly, two ambiguous SAR images are obtained with squint SAR algorithm. Then the Doppler ambiguity is solved by beam-forming [16]–[19] as a left-right angle resolution. The forward-looking azimuth angle resolution of this technique is only provided by the synthetic aperture, while the synthetic aperture in the forward-looking area contributes less to the azimuth angle resolution, resulting in lower azimuth angle resolution of the forward-looking area. Moreover, the binary array has low azimuth freedom, which is prone to singularities and makes it impossible to solve the Doppler ambiguity. (3) Monopulse forward-looking imaging technology, which achieves azimuth focusing of the signal component in a range bin by sum-difference angle estimation. The imaging performance is constrained by the monopulse angle estimation principle [20]–[22], which makes it impossible to distinguish multiple targets within a same beam. In a complex and low contrast scene, the imaging performance decreases rapidly. As a result, the direct application of these approaches to forward-looking SAR imagery encounter inherent difficulties. Some factors should be considered in forward-looking SAR under curve trajectory, which are listed as follows:

1) Forward-looking SAR imaging faces the problem of strong coupling of the range-azimuth, which leads to the difficulty of forward-looking SAR imaging. And different areas present different degrees of coupling. The closer to the trajectory, the stronger the range-azimuth coupling.

2) Synthetic apertures contribute differently to the azimuth angle resolution of different areas. As the target approaches the trajectory, the azimuth angle resolution contribution of the synthetic aperture is reduced, causing difficulty in forward-looking SAR imaging.

3) In actual flight, the trajectory usually has a certain curvature, which improves the azimuth angle resolution.

Considering the aforementioned factors, we propose a two-step processing algorithm to meet the demands of different processing methods in different regions. Compared with the above methods, the proposed algorithm has some innovations.

1) Compared with the conventional squint-looking SAR imagery, the proposed algorithm treats different areas in different ways due to the different degrees of coupling in different areas.

2) For the forward-looking-squint area, the system has a higher azimuth angle resolution and beam-forming can be used to solve the Doppler ambiguity. Therefore, the imaging method compatible with beam-forming is essential for forward-looking SAR imaging. The algorithm uses space-time cascading to ensure compatibility between beam-forming and SAR imaging. First, the ambiguous image can be obtained by the highly squinted-looking SAR imaging algorithm using time domain synthetic aperture resources. Then using the spatial domain array resources, beam-forming is performed to solve Doppler ambiguity.

3) For the forward-looking area, the azimuth angle resolution is insufficient and beam-forming cannot solve Doppler ambiguity. However, in actual flight, due to the influence of airflow and flight control system error, especially in missile applications, the trajectory usually has a certain curvature. This curvature would provide considerable diversity to improve the azimuth angle resolution of the forward-looking SAR. The proposed algorithm takes the benefit to the azimuth angle resolution from curve trajectory and develops a sparsity-driven optimization to improve the azimuth angle resolution.

In this paper, we first investigate the forward-looking multi-channel SAR (FLMC-SAR) model under the curve trajectory, which defines the azimuth direction as the vertical trajectory direction. The left-right Doppler ambiguity in FLMC-SAR system is analyzed, and an advanced algorithm using adaptive beam-forming is proposed to solve the Doppler ambiguity. The algorithm uses space-time cascading to ensure compatibility between beam-forming and SAR imaging. Second, FLMC-SAR azimuth angle resolution expression is presented with the wavenumber domain expression. The expression clearly indicates that the FLMC-SAR azimuth angle resolution is determined by both synthetic and real array apertures. It is emphasized that the curve trajectory is conducive to the enhancement of the azimuth angle resolution. A novel method through sparsity-driven optimization is carried out to exploit the curve trajectory for improvement of the azimuth angle resolution. Finally simulations are performed to validate the feasibility of the proposed algorithm.

The remainder of the paper is organized as follows: Section II gives the signal and geometry model of FLMC-SAR and a detailed description of the existing problem. Section III presents a clear description of the proposed algorithm. In Section IV, the experimental results are analyzed. In the final section, some crucial conclusions of this work are drawn.

II. FLMC-SAR SIGNAL MODEL AND PROBLEM DESCRIPTION

The FLMC-SAR geometry model is shown in Fig. 1. O_1X_1 is a straight trajectory and O_1QX_1 is a curved one. The angle between the track and the X-axis is the lower pressing angle ψ. The angle between the radar sight and the Z-axis is the beam pointing pitch angle α. The angle between the projection of the radar sight on the ground and the X-axis is the beam pointing azimuth angle θ. R_{X_i} is the uniform linear receiving antenna array, symmetrically distributed along the Y-axis over Y_1Y_2, and the antenna element spacing is d. T_X is the transmitting element, located at the midpoint of Y_1Y_2, overlapping with the central receiving antenna.

Firstly, we develop the signal model. Assume that there are two symmetric point targets P_1 and P_2 in the beam illumination area, which are symmetric about the X-axis, and their coordinates are $P_1(x_0, -y_0, 0)$ and $P_2(x_0, y_0, 0)$, respectively. The simultaneous coordinate of the transmitting element is defined by $(vt_m, 0, h(t_m))$, and a receiving element is at $(vt_m, y_i, h(t_m))$. Then the slant range equations of the

target (P_1 and P_2) are

$$\left.\begin{aligned} R_{Tx\_1}(t_m) &= \sqrt{(vt_m - x_0)^2 + y_0^2 + h(t_m)^2} \\ R_{Tx\_2}(t_m) &= \sqrt{(vt_m - x_0)^2 + y_0^2 + h(t_m)^2} \end{aligned}\right\} \quad (1)$$

$$\left.\begin{aligned} R_{Rx\_1}(t_m, y_i) &= \sqrt{(vt_m - x_0)^2 + (y_0 + y_i)^2 + h(t_m)^2} \\ R_{Rx\_2}(t_m, y_i) &= \sqrt{(vt_m - x_0)^2 + (y_0 - y_i)^2 + h(t_m)^2} \end{aligned}\right\} \quad (2)$$

where v represents the speed of the platform, t_m is the radar slow-time, $h(t_m)$ is the platform height, and y_i denotes the azimuth coordinate of the i-th receiving antenna. For a point target, the electromagnetic wave two-way slant range is

$$R(t_m, y_i) = R_{Tx}(t_m) + R_{Rx}(t_m, y_i) \quad (3)$$

The signal received by antenna can then be expressed as

$$\begin{aligned} s(\hat{t}, t_m, y_i) = A_P s_0(\hat{t}, t_m, y_i) &= A_P w_r\left(\hat{t} - \frac{R(t_m, y_i)}{c}\right) \cdot \\ &\times \exp\left[j\pi\gamma\left(\hat{t} - \frac{R(t_m, y_i)}{c}\right)^2\right] \cdot \\ &\times \exp\left[-j\frac{2\pi}{\lambda}R(t_m, y_i)\right] \\ &-\frac{D}{2} \le y_i \le \frac{D}{2} \end{aligned} \quad (4)$$

where A_P denotes the target scattering coefficient, $\hat{t}$ the radar fast-time, t_m the radar slow-time, $w_r(\hat{t})$ the range signal envelope, γ the Linear Frequency Modulation (LFM) rate, and D is the array antenna aperture size.

A. LEFT-RIGHT DOPPLER AMBIGUITY

From Eq. 1, it follows that $R_{Tx\_1}(t_m) = R_{Tx\_2}(t_m)$. The transmitting slant range R_{Tx} is independent of the array coordinate y_i, but the receiving slant range R_{Rx} is related to it. There is a difference in the receiving slant range between the symmetric point target P_1 and P_2 and their difference $\Delta R_{Rx} = R_{Rx\_1} - R_{Rx\_2}$. Let ΔR be the range resolution, which is much larger than ΔR_{Rx}. For the two point targets with symmetry of the trajectory, there is a difference between the two-way slant ranges of each channel, but the difference is too small to cause range cell migration. Therefore, the signals of P_1 and P_2 are mixed, which causes the left-right Doppler ambiguity of FLMC-SAR. The highly squinted-looking SAR imaging algorithm can obtain the ambiguous images. With this imaging result, beam-forming can be used to solve Doppler ambiguity. Therefore, the imaging method compatible with beam-forming is essential for forward-looking SAR imaging. In section III, Doppler ambiguity resolving via beam-forming will introudce in details.

B. FLMC-SAR SAR AZIMUTH ANGLE RESOLUTION ANALYSIS

FLMC-SAR achieves range high resolution by transmitting wide frequency bandwidth signals and pulse compression techniques, while the azimuth high resolution is provided by the synthetic aperture and the array real aperture. Theoretically, spatial resolution is directly determined by the corresponding wavenumber bandwidth. Here, the symbol θ denotes the beam pointing azimuth angle, D the real aperture length of the array antenna, L the projection of the trajectory on the plane XOZ, and r the reference slant range of the target. For the simplicity of azimuth angle resolution derivation, we define the target coordinate in the polar coordinate. Assume of $(r\sin\alpha\cos\theta, r\sin\alpha\sin\theta, 0)$ and $(X, Y, r\cos\alpha)$ are the coordinates of the point target and the antenna, respectively, and we have the slant range equation.

$$R = \sqrt{(X - r\sin\alpha\cos\theta)^2 + (Y - r\sin\alpha\sin\theta)^2 + r\cos\alpha^2} \quad (5)$$

Calculate the derivative of the slant range function with respect to $\sin\theta$.

The azimuth angle wavenumber is defined as

$$K_{\sin\theta}(X, Y) = \frac{\partial R}{\partial \sin\theta} \cdot K_{rc} \quad (7)$$

where K_{rc} is the range wavenumber center. With the relation of $r \gg X, r \gg Y$, we have $R \gg X, R \gg Y$, and the following approximations are valid.

$$\begin{aligned} K_{\sin\theta}(X, Y) = \frac{\partial R}{\partial \sin\theta} \cdot K_{rc} &\approx \frac{r\sin\alpha(X\tan\theta - Y)}{r} \cdot K_{rc} \\ &= \sin\alpha(X\tan\theta - Y) \cdot K_{rc} \end{aligned} \quad (8)$$

The azimuth angle wavenumber bandwidth is

$$\begin{aligned} \Delta K_{\sin\theta} &= \max\left(K_{\sin\theta}\right) - \min\left(K_{\sin\theta}\right) \\ &= \left[\tan|\theta|\left(X_{\max} - X_{\min}\right) + Y_{\max} - Y_{\min}\right] \cdot \\ &\quad \times \sin\alpha \cdot K_{rc} \end{aligned} \quad (9)$$

where $|\theta|$ is the absolute value of θ. According to the geometry shown in Fig. 1, we have

$$\left.\begin{aligned} X_{\max} - X_{\min} &= L\cos\psi \\ Y_{\max} - Y_{\min} &= D + \Delta y \end{aligned}\right\} \quad (10)$$

where Δy is the projection of the trajectory on the Y-axis direction. Then Eq. (9) can be written as

$$\Delta K_{\sin\theta} = \sin\alpha\left(\tan|\theta|\left(L\cos\psi\right) + D + \Delta y\right) \cdot K_{rc} \quad (11)$$

The azimuth angle resolution is

$$\begin{aligned} \Delta\left(\sin\theta\right) &= \frac{2\pi}{\Delta K_{\sin\theta}} \\ &= \frac{2\pi}{\sin\alpha\left(\tan|\theta|\left(L\cos\psi\right) + D + \Delta y\right) K_{rc}} \\ &= \frac{\lambda}{2\sin\alpha\left(\tan|\theta|\left(L\cos\psi\right) + D + \Delta y\right)} \end{aligned} \quad (12)$$

According to Eq. (12), the system azimuth angle resolution is provided by both synthetic and real array apertures. And the synthetic aperture is divided into two aspects, i.e., the synthetic aperture along the X-axis as a consequence of platform motion, denoted by $L\cos\psi$ and the synthetic aperture along the Y-axis due to the curve trajectory, denoted

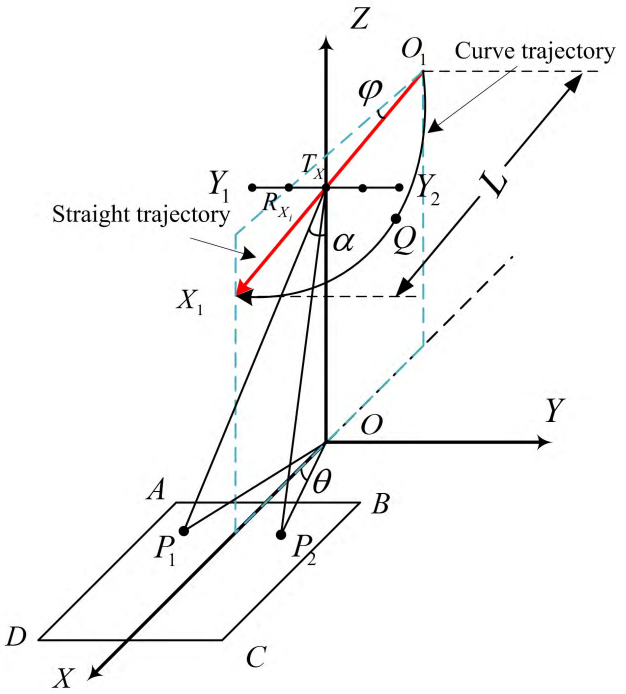

FIGURE 1. The FLMC-SAR geometry model.

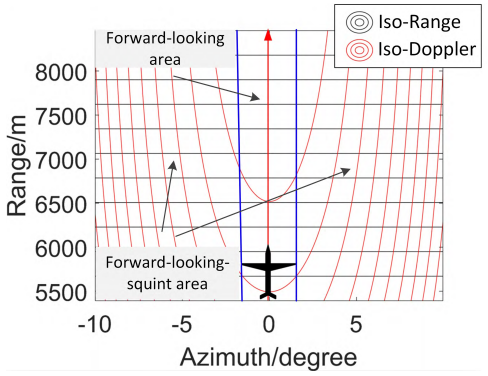

FIGURE 2. The equidistance and Doppler frequency grid.

by Δy. The $L\cos\psi$ contributes different azimuth angle resolution gain to areas at different azimuth angles. As the target approaches the trajectory, the azimuth angle resolution contribution of $L\cos\psi$ is reduced, causing difficulty in forward-looking SAR imaging. However, Δy is effective for the enhancement of the azimuth angle resolution in the forward-looking area.

The equidistance and Doppler frequency lines are shown in Fig. 2. One can notice that different areas present different degrees of coupling. The closer to the trajectory, the stronger the range-azimuth coupling and the more limited the azimuth angle resolution. In the forward-looking-squint area, the azimuth angle resolution is high enough to achieve focus imaging without Doppler ambiguity by beam-forming. However, the azimuth angle resolution of the forward-looking area is constrained by the size of real aperture. Limited resolution in the forward-looking area is not sufficient for the left-right Doppler ambiguity resolving with the beam-forming technique. Moreover, there is also a problem of strong coupling of the range-azimuth, which make the forward-looking SAR imaging a difficult task. Considering the benefit to the azimuth angle resolution from Δy, we propose a method to enhance the azimuth angle resolution of the forward-looking area in the next section.

III. TWO-STEP PROCESSING ALGORITHM

A. ALGORITHM FLOWCHART

Following the previous analysis, an advanced algorithm for FLMC-SAR imagery is introduced in this section, which treats different areas in different ways. As shown in Fig. 3, the approach runs a two-step process.

Step 1: For the forward-looking-squint area, the ambiguous images of each channel can be achieved by the highly squinted-looking SAR imaging algorithm. Then using the array spatial freedom, beam-forming is performed to solve the Doppler ambiguity.

Step 2: For the forward-looking area, with considering the contribution of the curve trajectory to the azimuth angle resolution, a sparsity-driven optimization imaging algorithm is developed to achieve the azimuth angle resolution enhancement.

Key steps are given in the following subsections.

B. LEFT-RIGHT DOPPLER AMBIGUITY RESOLVING

Aiming at the above-mentioned FLMC-SAR Doppler ambiguity problem, an advanced algorithm for Doppler ambiguity using beam-forming is proposed to achieve FLMC-SAR focus imaging without ambiguity. First, the signal is processed by the highly squinted-looking SAR imaging algorithm. Here, the back projection (BP) algorithm is utilized to achieve focus imaging with the Doppler ambiguity for each channel. Then using the spatial domain array resources, beam-forming is performed by weighting each channel image and accumulating coherently to solve the Doppler ambiguity. The algorithm adopts space-time cascading to ensure the compatibility between beam-forming and imaging.

$$\begin{aligned}\frac{\partial R}{\partial \sin\theta} &= \frac{-2r^2\sin^2\alpha\sin\theta + 2Xr\sin\alpha\tan\theta + 2r^2\sin^2\alpha\sin\theta - 2Yr\sin\alpha}{2\sqrt{(X - r\sin\alpha\cos\theta)^2 + (Y - r\sin\alpha\sin\theta)^2 + r\cos\alpha^2}} \\ &= \frac{r\sin\alpha(X\tan\theta - Y)}{\sqrt{(X - r\sin\alpha\cos\theta)^2 + (Y - r\sin\alpha\sin\theta)^2 + r\cos\alpha^2}}\end{aligned} \tag{6}$$

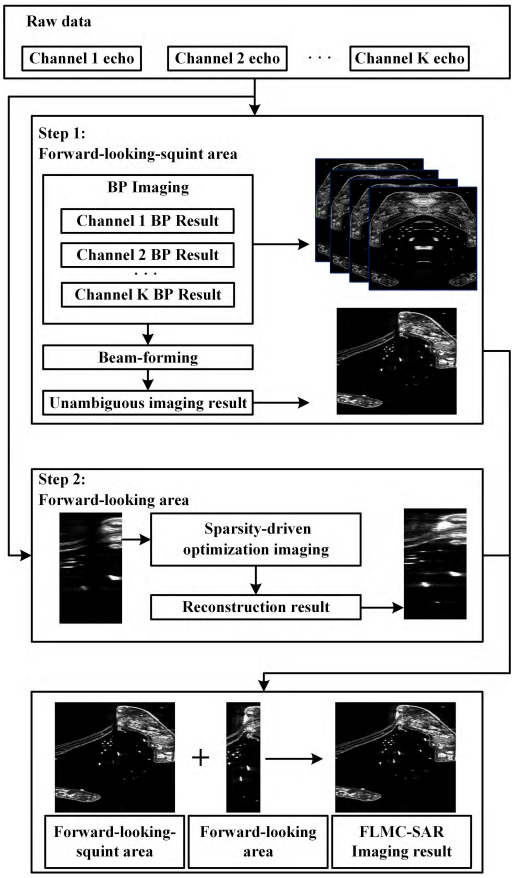

FIGURE 3. The flowchart of the proposed approach.

The signal is subjected to range pulse compression processing, and the pulse compressed signal can be expressed as

$$\begin{aligned} s_1(\hat{t}, t_m, y_i) &= IFFT\left\{FFT\left[s(\hat{t}, t_m, y_i)\right] \cdot FFT\left[s_{ref}(\hat{t})\right]\right\} \\ &= A_P \sin c\left[\pi B\left(\hat{t} - \frac{R(t_m, y_i)}{c}\right)\right] \cdot \\ &\quad \times \exp\left[-j\frac{2\pi}{\lambda}R(t_m, y_i)\right] \end{aligned} \tag{13}$$

where the symbol B denotes the signal bandwidth, *sinc* the sampling function, and $s_{ref}(\hat{t})$ the matching filter function.

$$s_{ref}(\hat{t}) = w_r(\hat{t}) \exp(-j\pi\gamma\hat{t}^2) \tag{14}$$

Next, BP imaging algorithm is performed, the essence of which is pixel reconstruction processing. Let the objective function $f(\rho, \theta)$ represent the reconstruction result of the point target $P(\rho\cos\theta, \rho\sin\theta)$.

$$f_P(\rho, \theta, y_i) = \sum\left\{s_1(\hat{t}, t_m, y_i)\exp\left[j\frac{2\pi}{\lambda}R(t_m, y_i)\right]\right\} \tag{15}$$

For the symmetry point targets $P_1(\rho\cos\theta, -\rho\sin\theta)$ and $P_2(\rho\cos\theta, \rho\sin\theta)$ with respect to the X-axis, the signal is ambiguous. As analyzed above, with the assumption that the delay of the symmetric target signal on the envelop is negligible, the BP result is

$$\begin{aligned} f_{P_1}(\rho, -\theta, y_i) = f_{P_2}(\rho, \theta, y_i) &\approx \begin{bmatrix} A_{P_1} \cdot s_0(\hat{t}, t_m, y_i) \\ A_{P_2} \cdot s_0(\hat{t}, t_m, y_i) \end{bmatrix}^T \cdot \\ &\quad \times \begin{bmatrix} \exp\left[j\frac{2\pi}{\lambda}R_{P_1}(t_m, y_i)\right] \\ \exp\left[j\frac{2\pi}{\lambda}R_{P_2}(t_m, y_i)\right] \end{bmatrix} \\ &= \begin{bmatrix} A_{P_1}A_{P_0} \cdot \exp\left[j\frac{2\pi}{\lambda}R_{P_1}(t_m, y_i - y_0)\right] \\ A_{P_2}A_{P_0} \cdot \exp\left[j\frac{2\pi}{\lambda}R_{P_1}(t_m, -y_0)\right] \end{bmatrix}^T \cdot \\ &\quad \times \begin{bmatrix} s_0(\hat{t}, t_m, y_i) \\ s_0(\hat{t}, t_m, y_i) \end{bmatrix} \end{aligned} \tag{16}$$

Here, $R_{P_1}(t_m, y_i)$ and $R_{P_2}(t_m, y_i)$ are the two-way slant range of the antenna with the array coordinate y_i to point P_1 and P_1. A_{P_0} is the phase delay from array center to point target, which is a constant independent of the steering vector.

$$A_{P_0} = \exp\left[j\frac{2\pi}{\lambda}R_{P_1}(t_m, 0)\right] = \exp\left[j\frac{2\pi}{\lambda}R_{P_2}(t_m, 0)\right] \tag{17}$$

Given the number of array elements K, the steering vector is

$$v(\theta) = \begin{bmatrix} \exp\left[j\frac{2\pi}{\lambda}y_1\sin(\theta)\right] \\ \exp\left[j\frac{2\pi}{\lambda}y_2\sin(\theta)\right] \\ \cdots \\ \exp\left[j\frac{2\pi}{\lambda}y_K\sin(\theta)\right] \end{bmatrix} \tag{18}$$

The reconstruction result at the grid corresponding to point targets P_1 and P_2 are the peak value of Eq. (16), which can be expressed as

$$\begin{aligned} F &= [f_{y_1}, f_{y_2}, \ldots, f_{y_K}]^T = \begin{bmatrix} f_{P_2}(\rho, \theta, y_1) \\ f_{P_2}(\rho, \theta, y_2) \\ \cdots \\ f_{P_2}(\rho, \theta, y_K) \end{bmatrix} \\ &= \begin{bmatrix} v(-\theta) & v(\theta) \end{bmatrix} \cdot \begin{bmatrix} A_{P_1}A_{P_0} \\ A_{P_2}A_{P_0} \end{bmatrix} = V \cdot A_p \end{aligned} \tag{19}$$

where F denotes the results of BP imaging of each channel, K the number of array elements, V the steering vector matrix, and A_p the scattering coefficient matrix of point targets with X-axis symmetry. In this paper, an advanced algorithm for Doppler ambiguity using adaptive beam-forming is proposed. The constraint of beam-forming is that it is required to form a zero point in the ambiguity direction, and the filtered signal is tightly coherent with the desired target steering vector. Under this constraint, the weights of a set of filters are solved and the output power of the array is minimized, which can be expressed as

$$\begin{cases} \min\limits_{W_k} J_{LCMP} \\ W_k^H V = g_k^H, k = 1, \ldots, K \end{cases} \tag{20}$$

The cost function representing the output power of the array J_{LCMP} is given by [21].

$$J_{LCMP} = E(\left|W_k^H X\right|^2) = W_k^H R_X W_k \tag{21}$$

Given the array receive signal X, the covariance matrix R_X, the steering vector matrix V, the dimension of the ambiguity N, (for the Doppler ambiguity problem of FLMC-SAR imaging, $N = 2$), and the k-th column of $N \times N$ identity matrix g_k, the optimal weight of the beam-forming can be determined.

$$W_k = {R_X}^{-1} V (V^H {R_X}^{-1} V)^{-1} g_k \tag{22}$$

According to the filter determined by this weight, beam-forming is performed by weighting each channel image and accumulating coherently to achieve focus imaging without Doppler ambiguity. Let $W = [W_1, W_2]$, and we can solve the scattering coefficient matrix.

$$W^H F = [W_1^H, W_2^H]^T V A_p = \begin{bmatrix} W_1^H V \\ W_2^H V \end{bmatrix} A_p = I A_p = A_p \tag{23}$$

C. SPARSITY-DRIVEN OPTIMIZATION IMAGING

According to the FLMC-SAR azimuth angle resolution analysis, synthetic aperture contribute differently to the azimuth angle resolution of different areas. As the target approaches the trajectory, the azimuth angle resolution contribution of the synthetic aperture is reduced and the coupling of range-azimuth increases, which causes difficulty in forward-looking SAR imaging. However, under the curve trajectory, the curvature will contribute to the azimuth angle resolution, which provides the possibility of high-resolution in the forward-looking area. Moreover, in actual flight, due to the influence of airflow and flight control system error, especially in missile applications, the trajectory usually has a certain curvature. Taking the azimuth angle resolution gain brought by the curve trajectory into consideration, a sparsity-driven optimization imaging algorithm is proposed to improve the azimuth angle resolution in the forward-looking area.

In FLMC-SAR imaging, different forward-looking areas present different Doppler frequencies. One can separate the echo of forward-looking area from that of forward-looking-squint areas by the bandpass Doppler filtering. Let S be the matrix of the pulse compressed echo of the forward-looking area in the same range bin, which contains K channels. And S could be written as

$$S_{KN} = [s_1(\hat{t}, t_m, y_1), s_1(\hat{t}, t_m, y_2), \ldots, s_1(\hat{t}, t_m, y_K)]_{KN} \tag{24}$$

where N donates the azimuth dimension of forward-looking area echo separated from the echo of forward-looking-squint area. The forward-looking area is divided into $\hat{N}$ units, that is, the angle is divided into $\hat{N}$ units, then Eq. (24) can be rewritten into the following linear measurement equation.

$$S_{KN\times 1} = F_{KN\times\hat{N}} A_{\hat{N}\times 1} + \epsilon_{KN\times 1} \tag{25}$$

where $A_{\hat{N}\times 1}$ is the scene high-resolution imaging result, $\epsilon_{KN\times 1}$ is the measurement noise, and F is the $KN \times \hat{N}$ measurement matrix, which represents the array manifold with the time-spatial diversity gained from both the synthetic aperture along the Y-axis Δy and the real aperture D.

$$F = [h_1, h_2, \ldots, h_{\hat{N}}] \tag{26}$$

Each of its columns corresponds to a steering vector in a different direction, expressed as

$$h_i = \begin{bmatrix} \exp\left[j\frac{2\pi}{\lambda} R(t_m, y_1)\right] \\ \exp\left[j\frac{2\pi}{\lambda} R(t_m, y_2)\right] \\ \cdots \\ \exp\left[j\frac{2\pi}{\lambda} R(t_m, y_K)\right] \end{bmatrix} \tag{27}$$

The spatial freedom of the steering matrix depends on Δy and the real aperture, which affects the forward-looking SAR imaging performance directly. The method of evaluating the measurement matrix is to analyze the cross-correlation properties between the column vectors. And small cross-correlations usually can guarantee the accuracy of sparse reconstruction underdetermined measurements. We define the spatial cross-correlation function to describe the spatial freedom of the steering matrix.

$$Corr(h_i, h_j) = \frac{\langle h_i^* \cdot h_j \rangle}{\|h_i\|_2 \|h_j\|_2} \tag{28}$$

where h_i and h_j are two column elements of the measurement matrix, $\langle\cdot\rangle$ is the inner product operation, $(\cdot)^*$ is the conjugate transpose operation, $\|\cdot\|_2$ is the l_2 norm,and $Corr$ is is the cross-correlation function. Under the curve trajectory, Δy will provide gain to the azimuth angle resolution, reduce the cross-correlation between the steering vectors, and improve the accuracy of the sparse reconstruction.

Assume that each element in noise matrix ϵ is independently submitted to the same Gaussian distribution with a mean of zero. Then the real part (ϵ_r) and the imaginary part (ϵ_i) of the noise ϵ are independent of each other and are submitted to the same real Gaussian distribution with a mean of zero. Let σ^2 be the variance of ϵ, then its Probability Density Function (PDF) is expressed as

$$\begin{aligned} P(\epsilon) &= \left[\frac{1}{(2\pi\sigma^2)^{\frac{KN}{2}}} \exp\left(-\frac{1}{2\sigma^2}\|\epsilon_r\|_2^2\right)\right] \cdot \\ &\quad \times \left[\frac{1}{(2\pi\sigma^2)^{\frac{KN}{2}}} \exp\left(-\frac{1}{2\sigma^2}\|\epsilon_i\|_2^2\right)\right] \\ &= \frac{1}{(2\pi\sigma^2)^{KN}} \exp\left(-\frac{1}{2\sigma^2}\|\epsilon\|_2^2\right) \end{aligned} \tag{29}$$

where, $\|\cdot\|_2$ denotes the l_2 norm, which is defined as $\|f\|_2^2 = \sum_i [f_i]^2$. Then the likelihood function corresponding to S is

$$P(S|A) = \frac{1}{(2\pi\sigma^2)^{KN}} \exp\left(-\frac{1}{2\sigma^2}\|S - FA\|_F^2\right) \quad (30)$$

Generally, sparsity is an inherent property of a target scene. According to the Compressed Sensing (CS), the Laplace distribution is used to characterize the sparsity of the target scene. So all the elements a_{nm} in A independently are submitted to the same Laplace distribution with positional parameter zero and scale factor γ. Then the PDF of a_n is

$$P(a_n) = \left(\frac{\gamma}{2}\right) \exp(-\gamma\|a_n\|_1) \quad (31)$$

where, $\|\cdot\|_1$ denotes the l_1 norm. Then, the PDF of A is expressed as

$$P(A) = \prod_{i=0}^{\hat{N}-1} \left(\frac{\gamma}{2}\right) \exp(-\gamma\|a_i\|_1) = \left(\frac{\gamma}{2}\right)^{\hat{N}} \exp(-\gamma\|A\|_1) \quad (32)$$

Define the l_1 norm of the matrix as $\|f\|_1 = \sum_{i=1}^{N} |f|_1$. Based on the Maximum A Posteriori (MAP) rule, the estimation function of A is

$$\hat{A}(S) = \arg\max [P(A|S)] \quad (33)$$

Based on the Bayesian rule, Eq. (33) can be rewritten as

$$\hat{A}(S) = \arg \max_{A \in C_{\hat{N}\times 1}} [P(S|A)\, P(A)] \quad (34)$$

By taking the logarithmic, Eq. (34) will be

$$\begin{aligned} \hat{A}(S) &= \arg \max_{A \in C_{\hat{N}\times 1}} \{\log [P(S|A)] + \log [P(A)]\} \\ &= \arg \max_{A \in C_{\hat{N}\times 1}} \left\{-\frac{1}{2\sigma^2}\|S - FA\|_F^2 - \gamma\|A\|_1\right\} \\ &= \arg \min_{A \in C_{\hat{N}\times 1}} \left\{\|S - FA\|_F^2 + 2\sigma^2\gamma\|A\|_1\right\} \\ &= \arg \min_{A \in C_{\hat{N}\times 1}} \left\{\|S - FA\|_F^2 + \mu\|A\|_1\right\} \end{aligned} \quad (35)$$

Assuming that the noise obeys the Gaussian distribution and the target image obeys the Laplace distribution, the above problem is equivalent to the l_1-constrained optimization problem, where $\mu = 2\sigma^2\gamma$ denotes the l_1-constrained coefficient, depending on the statistical parameters of the noise and the target distribution. The high-resolution imaging result of the forward-looking area can be reconstructed according to Eq. (35).

D. COMPUTATION COST

The proposed approach runs in a two-step process:

1) The Doppler ambiguity of BP image is solved by adaptive beam-forming. To perform BP imaging on a $N_G \times N_G$ grid with N_p pulses, we need $N_G^2 N_p$ times coherent accumulation. The total computation of the BP imaging of K channel is $O(KN_G^2N_p)$. In the beam-forming processing of $N_G \times N_G$ points image with K channel, there are $N_G/2$ times matrix inversion of size $K \times K$. The total computation of beam-forming processing is $O(K^3N_G)$.

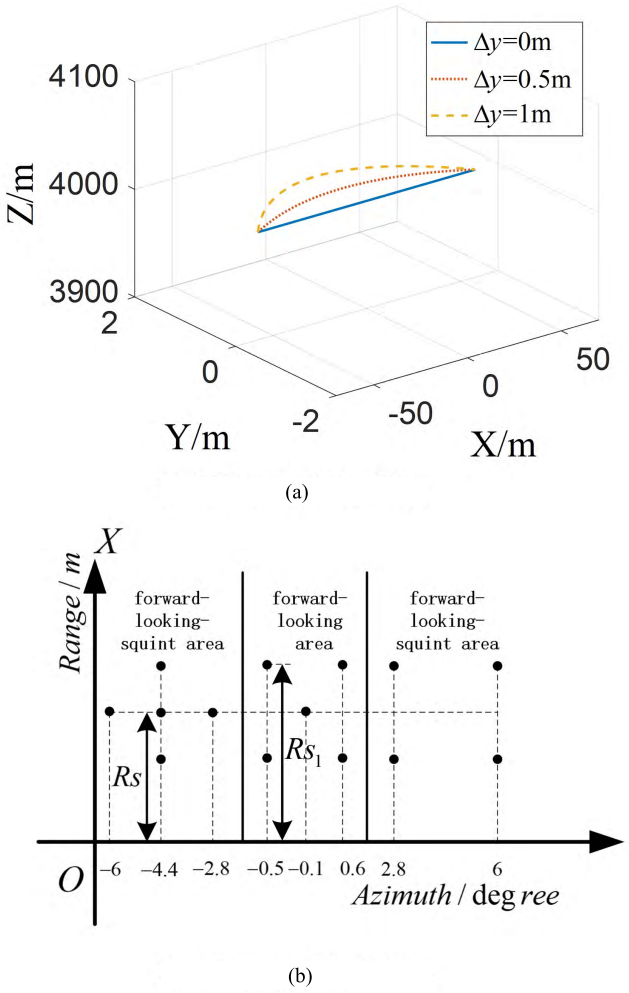

FIGURE 4. The Simulation parameters.

2) A sparsity-driven optimization imaging algorithm is developed to enhance the azimuth angle resolution in the forward-looking area. To achieve sparsity-driven optimization imaging on a $N_G \times N$ grid, we need N_G times sparse reconstruction with vector of size $N \times 1$. For the number of the iterations to achieve sparse reconstruction being N_{it}, we need N_{it} times matrix inversion of size $N \times N$. The total computation of sparse reconstruction is $O(N_G N_{it} N^3)$.

The total computation of the proposed method is $O(KN_G^2N_p + K^3N_G + N_G N_{it} N^3)$. The number of the channel K and the number of the iterations N_{it} is much smaller than the size of imaging grid N_G. Therefore, the computation complexity of the proposed method is determined by BP imaging, which is of order $O(KN_G^2N_p)$.

IV. EXPERIMENTS AND ANALYSIS

In order to demonstrate the performance and effectiveness of the proposed approach for forward-looking SAR imaging,

TABLE 1. Simulation parameters.

Parameter	Value	Parameter	Value
Carrier frequency	25GHz	PRF	8000Hz
Bandwidth	55MHz	Beam azimuth width	8degree
Number of array elements	5	Beam pitch width	22degree
Platform height	4000m	Real aperture length	0.4m

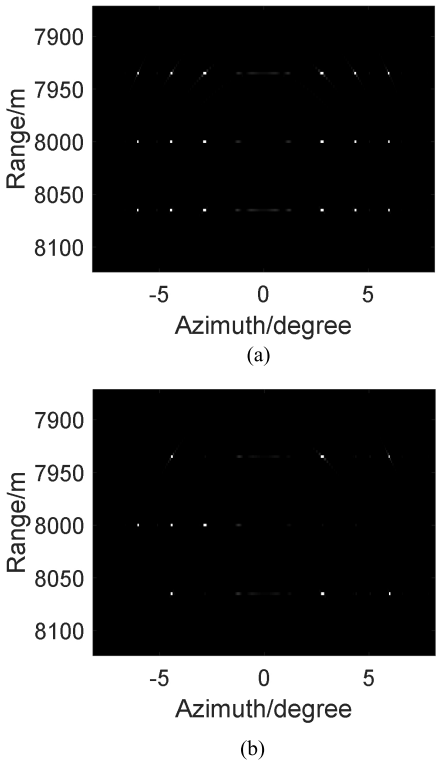

FIGURE 5. Imaging result of the forward-looking-squint area.

we perform different experiments to show its superiority from different aspects. The simulation experiment of the FLMC-SAR system under the curve trajectory is carried out. The curve trajectory is shown in Fig. 4(a), and the simulation parameters are shown in Table 1.

Part A: For the forward-looking-squint area, we perform a point target simulation to verify the compatibility of BP imaging and beam-forming.

Part B: For the forward-looking area, we analyze how Δy affects the reconstruction results. Based on the sparsity-driven optimization imaging algorithm, we perform a point target simulation experiment under the curve trajectory.

Part C: In order to further verify the effectiveness of the algorithm, we perform a synthetic simulation with multiple targets and extended scene. And the proposed two-step algorithm is utilized to achieve forward-looking SAR imaging.

A. BP IMAGING AND BEAM-FORMING

As shown in Table 1, the carrier frequency f_c is 25GHz and the real aperture length D is 0.5m, then the angle resolution

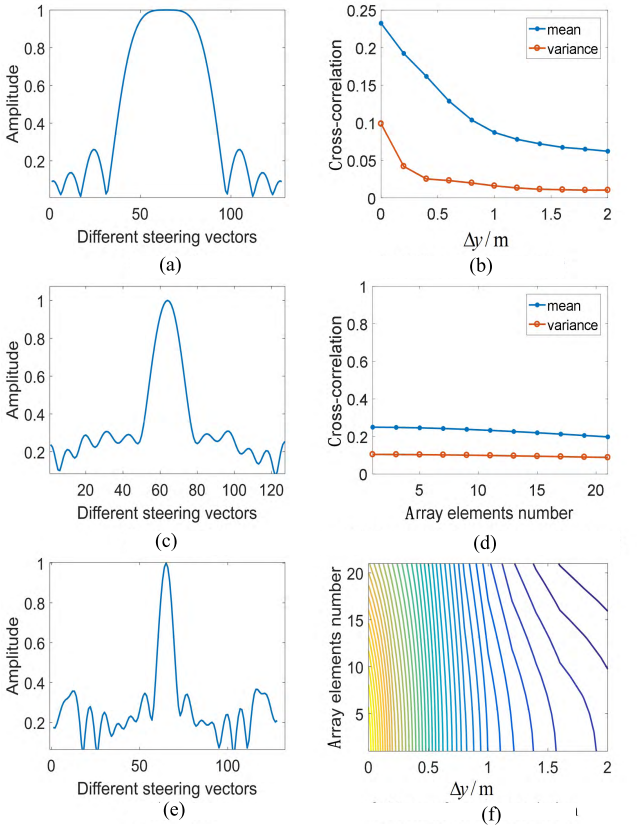

FIGURE 6. Cross-correlation of measurement matrix column vector under different values of Δy.

of the real aperture can be calculated as $C/fc/D = 1.71°$. For the area where $|\theta| \leq 1.71/2 \approx 1°$, the azimuth angle resolution is insufficient and beam-forming cannot solve Doppler ambiguity. Therefore we can define the area where $|\theta| \leq 1°$ as the forward-looking area and the area where $|\theta| > 1°$ as the forward-looking-squint area. In the point target simulation experiment, 14 point targets were placed in the imaging area as shown in Fig. 4(b). Here, the X-axis denotes the target reference slant range and the Y-axis denotes the target azimuth angle θ. There are 5 point targets in the forward-looking area and 9 point targets in the forward-looking-squint area. Fig. 5(a) shows the BP imaging result. As can be seen, the point targets can be distinguished clearly and well-focused. Apparently, the BP imaging result is symmetric about the center of the scene, which is caused by the Doppler ambiguity problem. We use beam-forming to solve the Doppler ambiguity problem of BP imaging result, and the result is shown in Fig. 5(b). By beam-forming, the forward-looking SAR imagery could be achieved without Doppler ambiguity. Clearly, the algorithm uses space-time cascading to ensure compatibility between BP imaging and beam-forming.

B. SPARSITY-DRIVEN OPTIMIZATION IMAGING

In this experiment part, we verify the effectiveness of the sparsity-driven optimization imaging algorithm in forward-looking area by comparing the imaging result of

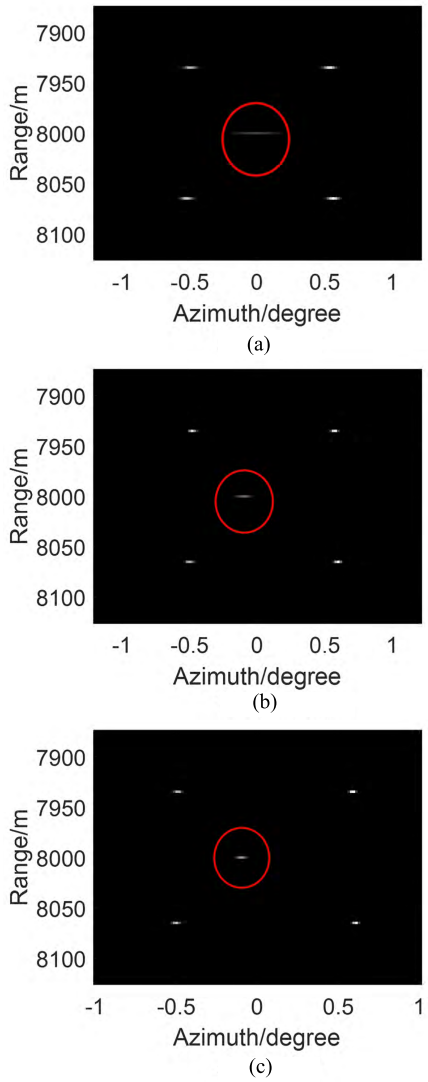

FIGURE 7. Sparsity-driven optimization imaging result. (a) $\Delta y = 0$m. (b) $\Delta y = 0.5$m. (c) $\Delta y = 1$m.

curve trajectory with different values of Δy. First of all, to analyze the impact of Δy on the reconstruction results, we give the cross-correlation characteristics between the different column vectors of the measurement matrix under the curve trajectory with different values of Δy.

Figs. 6(a), 6(b), and 6(c) are the cross-correlation of the measurement matrix for Δy of 0m, 0.5m, and 1m. Figs. 6(d), 6(e) and 6(f) show the variation of the mean and variance of the cross-correlation with different values of Δy and different numbers of array elements. It can be seen that no matter the number of array elements or the Δy increases, the cross-correlation of the measurement matrix decreases, which is beneficial to improving the accuracy of sparse reconstruction. However, the contribution of Δy or the number of array elements alone to the reconstruction of the forward-looking area is limited. Integrating the two aspects to maximize resource utilization is crucial.

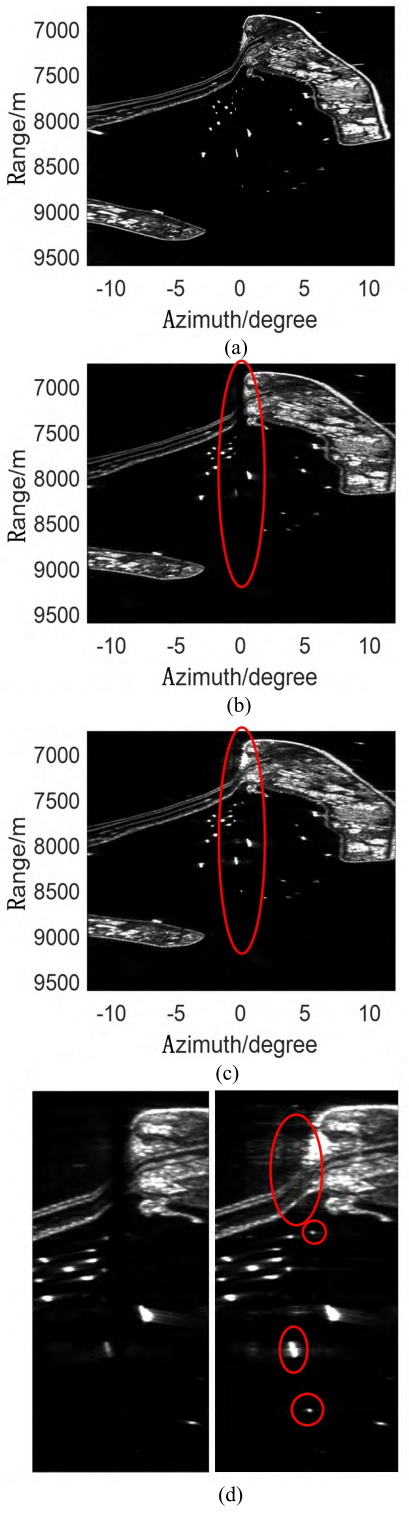

FIGURE 8. Surface target imaging result. (a) Reference image. (b) Forward-looking- squint imaging result. (c) Forward-looking imaging result. (d) Sparsity-driven optimization imaging result.

Then we give the sparsity-driven optimization imaging results with different values of Δy shown in Figs. 7. The resolution of the point target imaging results with different values of Δy are shown in Table 2. It clearly reveals that

TABLE 2. Resolution of the forward-looking area.

Resolution of the forward-looking area(m)			
Δy	(Rs,-0.1°)	(Rs_1,-0.5°)	(Rs_1,0.6°)
0m	28.51	6.08	6.91
0.5m	8.28	3.86	3.59
1m	4.64	3.48	3.31

as Δy increases the target resolution of the forward-looking area is improved. Especially the point target with an azimuth angle close to zero (highlighted in the figures by a circle), the resolution is improved significantly. Therefore, for the forward-looking area, the azimuth angle resolution gain due to the curve trajectory should be considered to enhance the resolution.

C. SYNTHETIC SIMULATION WITH MULTIPLE TARGETS AND EXTENDED SCENE

In order to further verify the feasibility of the method, a simulation experiment of surface target under the curve trajectory is carried out. The curve trajectory with Δy of 1m and the parameters are the same as shown in Table 1. The simulation uses the SAR image obtained by real data as a reference image, as shown in Fig. 8(a). High-resolution imaging of the forward-looking-squint area ($|\theta| > 1°$) can be performed by beam-forming, as shown in Fig. 8(b). However, beam-forming does not work for the forward-looking area ($|\theta| \leq 1°$), highlighted in Fig. 8(b) by a circle. The sparsity-driven optimization imaging method can achieve the target resolution of the forward-looking area, as shown in Fig. 8(c). The forward-looking area, highlighted in Figs. 8(b) and 8(c), is amplified in Fig. 8(d). The target of imaging failure in the forward-looking area by beam-forming are well reconstructed and can be distinguished clearly. The experiment validates our method for forward-looking SAR imagery.

V. CONCLUSION

Forward-looking SAR imaging faces the Doppler ambiguity and the difficulty of resolution caused by the strong coupling of the range-azimuth. The degree of coupling varies in different areas; Therefore, different treatments should be taken for different areas. For the forward-looking-squint area, beam-forming can be used to obtain high-resolution images without ambiguity. Thus, the imaging method compatible with beam-forming is essential for forward-looking-squint area. The space-time cascading algorithm proposed in this paper can guarantee the compatibility between beam-forming and SAR imaging. However, for the forward-looking area, beam-forming cannot be used to solve the Doppler ambiguity due to limited system resolution. But the curve trajectory will contribute to the azimuth angle resolution. Accounting for the contribution of the curve trajectory to the azimuth angle resolution, sparsity-driven optimization imaging processing can achieve high-resolution imaging results in the forward-looking area. The simulations indicate that a comprehensive use of beam-forming and sparsity-driven optimization imaging method can lead to high-resolution images of both forward-looking-squint and forward-looking areas.

REFERENCES

[1] S. A. Hovanessian, *Introduction to Synthetic Array and Imaging Radars*. Norwood, MA, USA: Artech House, 1980.
[2] J. P. Fitch, *Synthetic Aperture Radar*, New York, NY, USA: Springer, 1988.
[3] W. M. Brown and L. J. Porcello, "An introduction to synthetic-aperture radar," *IEEE Spectr.*, vol. 6, no. 9, pp. 52–62, Sep. 1969.
[4] W. G. Carrara, R. S. Goodman,R. M. Majewski, *Spotlight Synthetic Aperture Radar: Signal Processing Algorithms*. Norwood, MA, USA: Artech House, 1995.
[5] W. Pu, J. Wu, Y. Huang, J. Yang, W. Li, and H. Yang, "Joint sparsity-based imaging and motion error estimation for BFSAR," *IEEE Trans. Geosci. Remote Sens*, vol. 57, no. 3, pp. 1393–1408, Mar. 2019.
[6] W. Pu, J. Wu, Y. Huang, J. Yang, W. Li, and H. Yang, "A rise-dimensional modeling and estimation method for flight trajectory error in bistatic forward-looking SAR," *IEEE J. Sel. Topics Appl. Earth Observat. Remote Sens.*, vol. 10, no. 11, pp. 5001–5015, Nov. 2017.
[7] X. Z. Ren, J. T. Sun, and R. L. Yang, "A new three-dimensional imaging algorithm for airborne forward-looking SAR," *IEEE Geosci. Remote Sens. Lett.*, vol. 8, no. 1, pp. 153–157, Jan. 2011.
[8] J. Mittermayer, M. Wendler, and G. Krieger, "Data processing of an innovative forward looking SAR system for enhanced vision," in *Proc. Eur. Conf. Synth. Aperture Radar*, 2000, pp. 733–736.
[9] T. Sutor *et al.*, "Sector Imaging Radar for Enhanced Vision: Theory and applications," in *Proc. Eur. Conf. Synth. Aperture Radar*, 2000, pp. 357–359.
[10] W. Li, J. Yang, Y. Huang, and J. Wu, "A geometry-based Doppler centroid estimator for bistatic forward-looking SAR," *IEEE Geosci. Remote Sens. Lett.*, vol. 9, no. 3, pp. 388–392, May 2012.
[11] S. L. Dai and W. Wiesbeck, "The imaging mode of forward looking SAR with two receiving antennas," in *Proc. IEEE Int. Geosci. Remote Sens. Symp.*, Feb. 1999, pp. 1776–1778.
[12] W. Li, J. Yang, Y. Huang, L. Kong, and J. Wu, "An improved radon-transform-based scheme of Doppler centroid estimation for bistatic forward-looking SAR," *IEEE Geosci. Remote Sens. Lett.*, vol. 8, no. 2, pp. 379–383, Mar. 2011.
[13] H. S. Shin and J. T. Lim, "Omega-k algorithm for airborne forward-looking bistatic spotlight SAR imaging," *IEEE Geosci. Remote Sens. Lett.*, vol. 6, no. 2, pp. 312–316, Apr. 2009.
[14] X. Qiu, D. Hu, and C. Ding, "Some reflections on bistatic SAR of forward-looking configuration," *IEEE Geosci. Remote Sens. Lett.*, vol. 5, no. 4, pp. 735–739, Oct. 2008.
[15] H. Zhang, Y. Wang, and J. Li, "New applications of parameter-adjusting polar format algorithm in spotlight forward-looking bistatic SAR processing," in *Proc. APSAR*, Tsukuba, Japan, 2013, pp. 347–384.
[16] C. Zhou, Y. Gu, S. He, and Z. Shi, "A robust and efficient algorithm for coprime array adaptive beamforming," *IEEE Trans. Veh. Technol.*, vol. 67, no. 2, pp. 1099–1112, Feb. 2018.
[17] C. Zhou, Z. Shi, and Y. Gu, "Coprime array adaptive beamforming with enhanced degrees-of-freedom capability," in *Proc. IEEE Radar Conf.*, Seattle, WA, USA, Mar. 2017, pp. 1357–1361.
[18] Y. Gu *et al.*, "Coprime array adaptive beamforming based on compressive sensing virtual array signal," in *Proc. IEEE Int. Conf. Acoust., Speech, Signal Process.*, Shanghai., China, Jun. 2016, pp. 2981–2985.
[19] C. Zhou, Y. Gu, and W. Z. Song, "Robust adaptive beamforming based on DOA support using decomposed coprime subarrays," in *Proc. IEEE Int. Conf. Acoust., Speech Signal Process.*, Shanghai, China, May 2016, pp. 2986–2990.
[20] Y. X. Zhang *et al.*, "A novel monopulse angle estimation method for wideband LFM radars," *Sensors*, vol. 16, no. 6, pp. 817–825, Jun. 2016.
[21] Y. Yang and Y. L. Li, "A maximum likelihood extractor for forward-looking imaging of multiple unresolved targets in monopulse radar," in *Proc. CIE Int. Conf. Radar*, Guangzhou, China, 2016, pp. 1–4.
[22] M. Y. Fan, J. J. Ge, W. Qui, and M. Q. Wu, "Monopulse angle measurement for an airborne side-looking phased array PD radar," in *Proc. IEEE Radar Conf.*, Boston, MA, USA, Feb. 2007, pp. 209–211.

JINGYUE LU was born in Hebei, China, in 1994. He received the B.S. degree in communication engineering from the Ocean University of China, Qingdao, China, in 2016. He is currently pursuing the Ph.D. degree in signal processing with the National Laboratory of Radar Signal Processing, Xidian University. His research interest includes radar imaging.

LEI ZHANG was born in Zhejiang, China, in 1984. He received the Ph.D. degree from Xidian University, in 2012, where he is currently an Associate Professor with the National Laboratory of Radar Signal Processing. He is also with the School of Electronics and Communication Engineering, Sun Yat-sen University. His research interests are radar imaging (SAR/ISAR) and motion compensation.

PENGFEI XIE was born in Henan, China, in 1992. He received the B.S. degree in electronic information science and technology from the Qingdao University of Technology, Qingdao, China, in 2016. He is currently pursuing the master's degree in signal processing with the National Laboratory of Radar Signal Processing, Xidian University. His research interest includes radar imaging.

ZHICHAO MENG was born in Shaanxi, China, in 1997. He received the B.S. degree in remote sensing from Xidian University, Xi'an, China, in 2015, where he is currently pursuing the master's degree in signal processing with the National Laboratory of Radar Signal Processing. His research interest includes radar imaging.

YUNHE CAO was born in Anhui, China. He received the B.S., M.S., and Ph.D. degrees from Xidian University, Xian, China, in 2001, 2004, and 2006, respectively, where he is currently a Professor with the National Laboratory of Radar Signal Processing. His research interests include MIMO radar, digital array radar, adaptive signal processing, and target detection.